

RSC Advances



This is an *Accepted Manuscript*, which has been through the Royal Society of Chemistry peer review process and has been accepted for publication.

Accepted Manuscripts are published online shortly after acceptance, before technical editing, formatting and proof reading. Using this free service, authors can make their results available to the community, in citable form, before we publish the edited article. This *Accepted Manuscript* will be replaced by the edited, formatted and paginated article as soon as this is available.

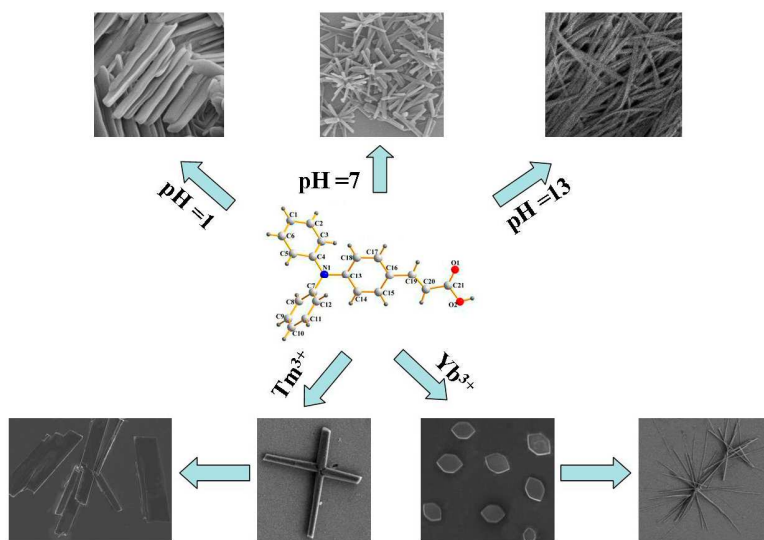
You can find more information about *Accepted Manuscripts* in the [Information for Authors](#).

Please note that technical editing may introduce minor changes to the text and/or graphics, which may alter content. The journal's standard [Terms & Conditions](#) and the [Ethical guidelines](#) still apply. In no event shall the Royal Society of Chemistry be held responsible for any errors or omissions in this *Accepted Manuscript* or any consequences arising from the use of any information it contains.

Graphic abstract for:

Self-aggregation of fluorophore-triphenylamine nanostructures with tunable luminescent properties: effect of acidity and rare earth ions

Qi-yu Chen, Lin Kong, Yu-peng Tian, Long-Mei Yang, Gao-bin Zhang, Wen-bin Jia, Jia-xiang Yang



A D- π -A type triphenylamine derivative, **L**, is synthesized and characterized by single crystal X-ray diffraction analysis. The self-aggregation of **L** nanostructures in different acidity aqueous solution and/or under guidance of rare earth ions is studied to optimize the optical properties.

Cite this: DOI: 10.1039/c0xx00000x

www.rsc.org/xxxxxx

Self-aggregation of fluorophore-triphenylamine nanostructures with tunable luminescent properties: effect of acidity and rare earth ions

Qi-yu Chen,^a Lin Kong,^{a*} Yu-peng Tian,^{a,b} Xian-yun Xu,^a Long-Mei Yang,^a Gao-bin Zhang,^a Wen-bin Jia,^a Jia-xiang Yang^{a,b*}

Received (in XXX, XXX) Xth XXXXXXXXX 20XX, Accepted Xth XXXXXXXXX 20XX

DOI: 10.1039/b000000x

A D- π -A type triphenylamine derivative 3-(4-(diphenylamino)phenyl)acrylic acid (abbreviated as **L**) is designed, synthesized and characterized by single crystal X-ray diffraction analysis. The self-aggregation of **L** nanostructures in different acidity aqueous solution and/or under guidance of rare earth (RE) ions is studied, along with the corresponding optical properties. In strong acidic conditions, **L** molecules self-assemble to form two dimensional nanostructures. While in neutral aqueous solution, **L** tends to form nanorods. In the strong alkali environment, nanofibers were obtained. Moreover, in acidic conditions, the existence of Tm^{3+} induces **L** molecules self-aggregate into nanoplates. Flower-like six branched structures are observed when Yb^{3+} is used, respectively. The changed morphology leads to tunable linear optical properties.

1 Introduction

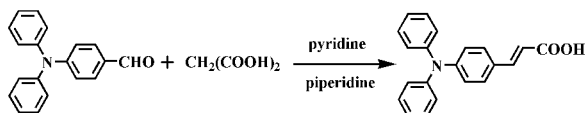
Over the past few decades, increasing interest has been received about functional organic materials composed of optically and electronically active constituents in nanoscience and nanotechnology [1-3]. The tunable physical properties of organic nanomaterials can be controlled through their size, shape and crystallinity, which are expected to provide an opportunity to control optoelectronic properties and further device performance [4-6]. Multitude of cooperative and simultaneous intermolecular interactions, such as hydrogen bonding, van der Waals, π - π stacking and electrostatics attraction, can affect the final structure and further adjust the corresponding properties [7-9]. In addition, the concentration, temperature, surfactants, solution acidity can also be used to alter or control above-mentioned interactions and further cause the change of morphology [10-13]. However, to the best of our knowledge, little research has been carried about using RE metal ions to induce and/or control the morphology and/or particle size of an organic nanostructure.

Rare earth ions have been extensively studied in the fundamental and technical field over the past decades due to their particular characteristics arising from the 4f and/or 5f electronic shells [14-15], which have great potential to be used in luminescent devices, magnets, catalysts and other functional materials [16-18]. Compounds consisting of RE ions also have significant commercial applications in radiation intensifying screens, X-ray-computed tomography, oxygen storage, and medical imaging radiation detectors [19-20]. It is well known that

there are significant magnetic interactions between carboxylate compounds and the RE ions [21]. According to the Hard-Soft Acid-Base principle, RE ions should have high tendency to combine with O atoms of these carboxylate compounds. Thus, the interactions between the RE ions and oxygen atom of carboxylate ligands are somewhat strong. Up to now, the usage of RE ions as the efficient inductive agent to build the organic nanostructures is rarely reported. Therefore, in this study, the interaction between RE ion and carboxylate derivative is used to regulate the morphology.

In many functional organic materials, triphenylamine and its derivatives are well-known for their 3-D propeller shapes which have been widely investigated and applied in organic field-effect transistors, organic light-emitting diodes, as well as second order nonlinear optical devices [22-24]. In many cases, triphenylamine groups can be employed as electron-donors and used to prepare D- π -A type molecules (D = donor, A = acceptor) through linkage with an electron-acceptor group, which are regarded as ideal candidates for red emitting and nonlinear optical materials [25-26]. To increase the interactions between RE ions and organic matrix, carboxylic group is introduced into triphenylamine group, which can also improve the solubility of the as-prepared organic compound in water as well and further present a bright future for the application.

Considering all the aspects above, in this work, an ICT structural triphenylamine derivative, **L** (Scheme 1), was designed and synthesized, in which triphenylamine group was employed as electron-donor unit and the carboxyl group as an electron-acceptor unit. Further, nanostructures of **L** were prepared under



Scheme 1 Synthetic routes of the target compound L

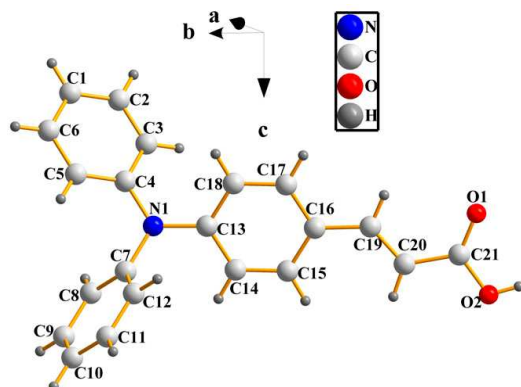


Fig. 1 Crystal structure of L with the atom numbering scheme

different conditions. The influence of solution acidity (pH) and Tm^{3+} , Yb^{3+} ions on the morphology and the corresponding linear optical properties of L were discussed. It is found that pH plays an important role in the formation of the morphology. The morphology of L has a tendency to accumulate form semi two dimensional nanostructure in the excessive acid environment and one dimensional nanorods in neutral aqueous solution. However, in the alkaline solution, the surface of L nanostructures was etched due to the acid-base reaction and eventually nanofibers were observed. Further, the interactions between L and RE ions through a simple process at room temperature result in completely different morphology. In brief, by controlling the acidity of solution and RE metal ions, self-assembly of 1-D or semi 2-D organic materials can be achieved. The existence of Tm^{3+} induces nanoplates in acidic condition. Flower-like six branched structure is obtained when Yb^{3+} is used.

2. Experimental Section

2.1 Materials and Instrument

All reagents used in synthesis route were of analytical reagent grade. The pH of the solution was adjusted by adding hydrochloric acid or sodium hydroxide in water and demarcated with the pH meter of PHS-3CT. Metal salts $\text{Tm}(\text{NO}_3)_3 \cdot 5\text{H}_2\text{O}$, $\text{Yb}(\text{NO}_3)_3 \cdot 5\text{H}_2\text{O}$ were prepared from the corresponding metal oxidate and concentrated nitric acid.

The X-ray diffraction measurement of single crystal was performed on a Bruker SMART CCD area detector using graphite-monochromated Mo K α radiation ($\lambda = 0.71073 \text{ \AA}$) at 298(2) K. Intensity data were collected in the variable ω -scan mode. The structures were solved by direct methods and difference Fourier syntheses. All non-hydrogen atoms were refined anisotropically and hydrogen atoms were introduced geometrically. Calculations were performed with the SHELXTL-97 program package [27]. The morphologies were obtained on a field-emission scanning electron microscope (FESEM, Hitachi S-4800). UV-vis absorption spectra were obtained on a UV-3100 spectrophotometer in the wavelength range 200-700 nm.

Fluorescence spectra were measured at room temperature using a Hitachi F-7000 spectrophotometer.

2.2 Synthesis of L

4-(diphenylamino)benzaldehyde (0.5g, 1.8mmol) and malonic acid (0.0187 g, 1.8 mmol) were dissolved in pyridine (5 mL) and 3-5 drops of piperidine was added as a catalyzer. The above mixture was refluxed for 4 h at 90 °C and monitored by TLC to ensure complete reaction. Then, water was added to the mixture, the precipitate was purified through recrystallization in ethanol solution to get a yellow solid. Yield: 95%. ^1H NMR (400MHz, d_6 -DMSO): δ (ppm) 12.22 (s, 1H); 7.56 (d, 2H, $J = 6.8$ Hz); 7.50 (d, 1H, $J = 16.0$ Hz); 7.36 (t, 4H, $J = 7.6$ Hz); 7.13 (t, 2H, $J = 7.2$ Hz); 7.09 (d, 4H, $J = 8.0$ Hz); 6.89 (d, 2H, $J = 8.0$ Hz); 6.34 (d, 1H, $J = 16.0$ Hz); ^{13}C NMR (100MHz): δ (ppm) 167.54, 146.34, 143.49, 129.75, 129.54, 127.21, 125.01, 124.15, 120.93, 116.39. FT-IR (KBr, cm^{-1}): $\nu = 3029(\text{m}, \nu_{\text{COO}})$, 1681 (s, $\nu_{\text{C=O}}$), 1622 (w, $\nu_{\text{C=C}}$), 1584 (s), 980 (w), 829 (w), 753(m), 698(s).

Yellow crystals of L suitable for X-ray diffraction were obtained by slow evaporation of dichloromethane-methanol mixed solution ($V_{\text{CH}_2\text{Cl}_2} : V_{\text{MeOH}} = 2:1$) at room temperature for a week.

2.3 Preparation of aggregates

Stock ethanol solution of L with a concentration of $1.0 \times 10^{-3} \text{ mol}\cdot\text{L}^{-1}$ was prepared. Stock aqueous solutions of different acidity (pH values of which were 1, 3, 4, 5, 7, 9 and 13, respectively) and stock aqueous solutions of RE ions (Tm^{3+} , Yb^{3+}) were also prepared.

The organic nanostructures were prepared through a simple reprecipitation process. In details, 200 μL of L-ethanol solution was injected into 2 mL of high-purity water under stirring. For studying the effect of acidity on the aggregation, 200 μL of L-ethanol solution was injected into 2 mL of high-purity water with different acidity under stirring. For exploring the effect of RE ions on the aggregation, the aqueous solution of Tm^{3+} and/or Yb^{3+} was rapidly added into 2 mL of high-purity water and/or aqueous solutions with different acidity with stirring for 3 min. Then, 200 μL of L-ethanol solution was injected into the above solution under stirring. The samples were stirred for 10 min and then left undisturbed for 12 h at room temperature for stabilization.

2.4 TD-DFT calculation

Molecular orbital calculations of time-dependent density functional theory (TD-DFT) at the pbe1pbe/6-31g level basis set (Gaussian 09) were performed to study the electronic structures of L [28]. The molecular geometry used for the calculation was obtained from X-ray diffraction crystallographic data.

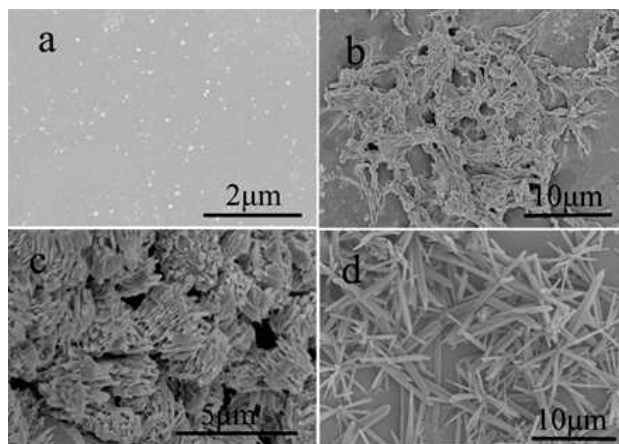
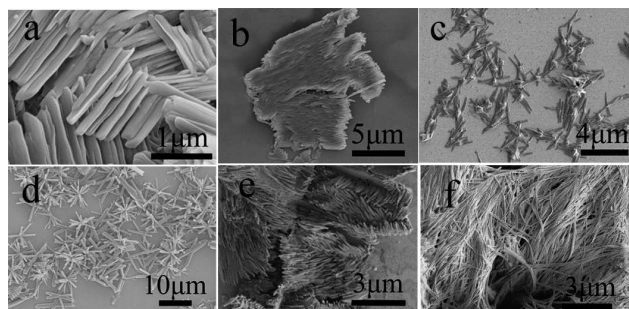
3. Results and discussion

3.1 Structural Characterization

L crystallized in monoclinic form with space group $P2(1)/n$ as shown in Fig. 1. The crystallography data is summarized in Table 1. Selected bond lengths and bond angles are listed in ESI Table S1. In the molecule, the bond lengths were all of aromatic character. The linkage bond length between the benzene ring and the carboxyl group was quite conjugated with C16-C19 being

Table 1 Crystal data and structure refinement for **L**

empirical formula	C ₂₁ H ₁₇ NO ₂	a [Å]	13.716(5)
formula weight	315.36	b [Å]	8.084(5)
crystal system	monoclinic	c [Å]	15.868(5)
space group	P2(1)/n	β [deg]	100.602(5)
temperature (K)	298(2)	V [Å ³]	1729.4(14)
Z	4	D _{calcd} [g·cm ⁻³]	1.211
F(000)	664	goodness of fit on F ²	1.032
Crystal size (mm)	0.30 × 0.20 × 0.20	Reflections collected / unique	2366
Final R indices [I>2σ(I)]	R ₁ = 0.0409, wR ₂ = 0.1329	R indices (all data)	R ₁ = 0.0549, wR ₂ = 0.1497

**Fig. 2** The morphologies of **L** from different mixed solvents: (a) DMF-H₂O, (b) acetonitrile-H₂O, (c) acetone-H₂O, (d) ethanol-H₂O.**Fig. 3** SEM images of **L** nanostructures prepared in aqueous solution with different acidity (a) pH = 1, (b) pH = 3, (c) pH = 5, (d) pH = 7, (e) pH = 9, (f) pH = 13.

1.399(12) Å. The C19=C20 double bond was nearly coplanar to the adjacent benzene and carboxyl group with the torsion angle of C17-C16-C19-C20 being 176.01(16)° and O2-C21-C20-C19 being 179.90(15)°. The structural features suggested that all nonhydrogen atoms were highly conjugated and nearly coplanar, which would favour the electronic delocalization in the whole molecule.

The adjacent molecules are stacked through C-H...C weak interactions along the same direction (*b* axis) at a short intermolecular distance between 2.804-2.854 Å to form 1-D structure as shown in Fig. S1a. There is also a O2-H2...O1 intermolecular hydrogen bond with the H...O distance of 1.842 Å (C-H...O = 178.59°), which is very important in supramolecular

crystal packing to form 2-D sheets in the *ab* plane (Fig. S1b). There also exists a C10-H10...O1 intermolecular hydrogen bond with the H...O distance of 2.349 Å (C-H...O = 163.56°), which connects with C-H...C weak interactions mentioned above to form 2-D sheets in the *bc* plane. Such strong weak interactions were supposed to be the main driving forces for the molecules self-assembly along a certain direction to form bulk materials and/or nanomaterials.

3.2 Effect of solvent on the aggregation of **L**

In the present work, **L** nanostructures are simply prepared in several solvents with no addition of any surfactant, template or catalyst. SEM images of **L** self-assembly aggregations from different solvents are shown in Fig. 2. The solvent-induced morphological change of **L** is remarkable. Monodisperse spherical nanoparticles are observed in DMF-H₂O mixed solvent with average diameter of about 80 nm and good dispersion (Fig. 2a). Nanobelts are observed in acetonitrile-H₂O with the length about 10 μm and the width about 500 nm (Fig. 2b) which have tendency to aggregate. The main product in acetone-H₂O is nanorod with the length about 1.3 μm and the average width of about 140nm (Fig. 2c), which are directional arranged one by one. Moreover, nanorods with lengths of about 10 μm and the average width of about 200 nm are obtained in ethanol-H₂O (Fig. 2d). This solvent-based morphology variation can be attributed to the different intensity of noncovalent intermolecular interactions between **L-L** and **L-solvent** [29]. Owing to the fact that the morphology of **L** obtained from ethanol was more irregular than that from the other solvents, the following experiments were carried out in ethanol solution in this work.

3.3 Effect of acidity on the aggregation of **L**

As **L** is a carboxylic acid derivative, the acidity of the solution may change the weak intermolecular interactions and further influences the morphology. In order to study the influence of acidity of the solution on the morphology, experiments were conducted by adjusting the acidity of EtOH/water mixed solution as shown in Fig. 3. When the experiment was carried out at neutral conditions of pH = 7, nanorods with smooth surface were observed with lengths and diameters of ~10 μm and ~200 nm respectively (Fig. 3d), which fit well with the result shown in Fig. 2d.

As the acidity of solution varied, a remarkable change of **L** self-aggregation was observed. When the acidity of solution increased, the morphology gradually changed from nanorods to ordered superimposed flake-like semi 2-D structures. In detail, when the acidity was pH = 5 (Fig. 3c), there is a slight change in the morphology compared to that of the neutral condition. The nanorods in decentralized state were appeared with the length decreased to ~1.5 μm. When the acidity increased to pH = 4, two different morphologies of stacked structure and dispersed nanorods coexisted (Fig.S2). The stacked structure made of multiple nanorods arranged orderly with the length about 3 μm and the thickness about 1.5~2 μm. The dispersed nanorods had an average length about 4 μm. The results indicated that the driving force of the formation of different nanostructure was probably a complex balance of intermolecular interactions.

Further, as the acidity increased to pH = 3, aggregated nanorods were observed to form semi 2-D structure (Fig. 3b). The

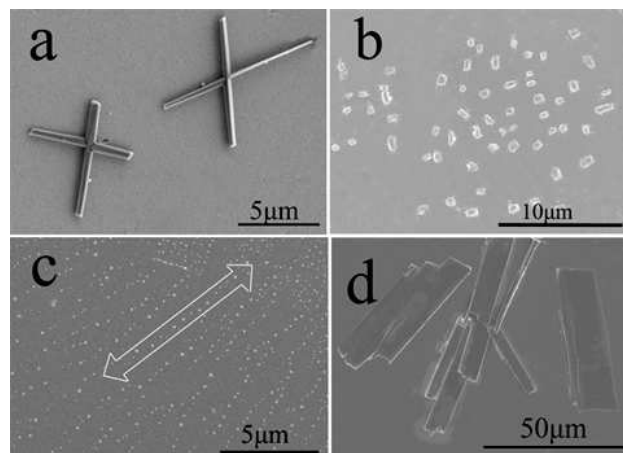


Fig.4 SEM images of nanostructures of **L** with the $\text{Tm}(\text{NO}_3)_3 \cdot 5\text{H}_2\text{O}$: in the aqueous solution and the concentration of Tm^{3+} is 4×10^{-4} M (a), in the acidic aqueous solution of pH = 3 and the concentration of Tm^{3+} is 2×10^{-6} M (b); 6×10^{-6} M (c); 2×10^{-5} M (d) respectively, and virtual arrow inset of c is the virtual direction.

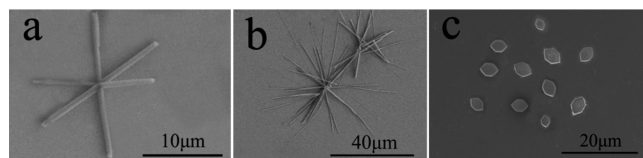


Fig.5 SEM images of nanostructures of **L** with the $\text{Yb}(\text{NO}_3)_3 \cdot 5\text{H}_2\text{O}$: (a) in the aqueous solution and the concentration of Yb^{3+} is 8×10^{-5} M, (b) in the aqueous solution and the concentration of Yb^{3+} was increased to 2×10^{-4} M. (c) in the acidic aqueous solution of pH = 3 and the concentration of Yb^{3+} is 6×10^{-5} M.

length and diameter of a single nanorod were $\sim 1 \mu\text{m}$ and 200 nm , respectively. These nanorods gathered to form semi 2-D structure with $\sim 20 \mu\text{m}$ length and $\sim 15 \mu\text{m}$ width. The border between the adjacent nanorods was clearly observed, which showed the aggregation and weak intermolecular interactions along two directions. When the acidity of the preparation environment increased to pH = 1, a superimposed flake-like structures were obtained (Fig. 3a). A single nanoflake possessed a width of about 300 nm , thickness of $70\text{--}80 \text{ nm}$ and average length of about $1.2\text{--}1.6 \mu\text{m}$. Several nanoflakes stacked closely and the interface was clearly observed. The nanoflake had high morphological purity as other morphology was seldom captured under such condition.

Another interesting trend of morphology change was observed when **L** molecules were put in alkaline medium. When the acidity of the aqueous solution reached to pH = 9, one-armed nanotubes was obtained (Fig. 3e) with the length of about $3\text{--}5 \mu\text{m}$ and the average bore diameter being 100 nm . The formation of one-armed nanotubes was considered as coming from the erosion effect on the nanorods. The surface of the nanotubes was rough, which may be due to the erosion effect caused by the interactions between alkali and carboxylic group. These one-armed nanotubes arranged orderly and stacked into a quasi 2-D structure. Further, when the acidity reached to pH = 13, nanofibers arose with length of $\sim 30 \mu\text{m}$ and width about 200 nm (Fig. 3f), which was marked distinction compared with the nanorods obtained in pH = 7. Moreover, the growth direction of these nanofibers was basically the same in the visual field, which revealed that the

intermolecular interactions along this direction were the main driving forces to form the nanofibers.

When **L**-EtOH solution was injected into pure water, the sudden change in the environment of **L** molecules induced molecular segregation from ethanol and precipitation in water to form seed crystals. In the subsequent growth process, the strong intermolecular D-A dipole-dipole interactions between adjacent **L** molecules acted as the driving force for the aggregation of **L** molecules. The limited solubility of **L** in the poor solvent (water), together with the strong intermolecular dipole-dipole interactions, drove **L** molecules to align orderly and assemble mainly along the direction of the dipole moment, and thus 1-D nanorods were formed.

While in the acid solution, the carboxylic acid unit of **L** was fully protonated. Thus, the hydrogen bond between the carboxyl groups of **L** and water would be stronger. The process would decrease the probability of the formation of O-H---O hydrogen bonds. Thus, the proportion and the corresponding strength of the C-H---C weak interactions between triphenylamine group and $\pi\text{-}\pi$ weak interactions between conjugated groups of adjacent molecules would increase and be comparable to that of O-H---O hydrogen bonds. The three types of weak interactions would be the main driving force for the molecular packing and led to the creation of accumulation from 1-D morphology to 2-D structures [30]. However, when the environment changed to alkaline condition, the carboxyl group was expected to be deprotonated, which caused the intermolecular hydrogen bond weakened and even disappeared. Thus, the C-H---C weak interactions was dominant in the molecular self-assembly, resulting in more obviously 1-D orientational growth [31].

3.4 Morphology of **L** nanostructure induced by RE ions

Through the above study, it is concluded that solvent and acidity of the solution have significant effect on the self-aggregation of **L** molecules. Further, the effect of RE metal ions on the morphology of **L** was studied. A more interesting change on the morphology was expected based on the strong interactions between RE metal ions with O atoms of **L**. To explore the aim, the aqueous solution of Tm^{3+} (4×10^{-4} M) was added to the reaction system. A cross-like structure was observed, which had a length of about $6\text{--}10 \mu\text{m}$ and the larger angle made of two nanorods was about 100° (Fig. 4a). As the concentration of Tm^{3+} increased, the molecular interactions of a certain direction enhanced and led to the increased length of the nanorods and a small quantity of impurities. The phenomenon possibly caused by the hydrolysis of Tm^{3+} (Fig. S3). In order to eliminate this hydrolysis effect, the solution was adjusted to acidic conditions. When Tm^{3+} ions were added into the acidic aqueous solution, the morphology of **L** further changed. For example, when the sample was prepared in pH = 3 and the concentration of Tm^{3+} was 2×10^{-6} M, unordered rectangular nanoplates were obtained (Fig. 4b). However, as the concentration of Tm^{3+} gradually increased to 6×10^{-6} M, the nanoplate structures grew along a particular direction shown in Fig.4c (the white solid lines is the virtual growth direction of the nanostructures). When the concentration of Tm^{3+} increased to 2×10^{-5} M, the nanoplate structure finally grew into a large size sheet-like structure with the length about $30\text{--}50 \mu\text{m}$ and width about $4\text{--}20 \mu\text{m}$ (Fig. 4d).

To further explore the influence of different RE ions on the

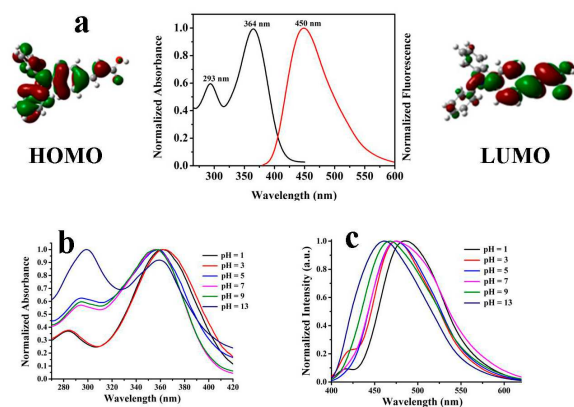


Fig.6 The UV-vis spectra of **L** measured in ethanol and spatial distributions of the calculated HOMO and LUMO (a), UV-vis (b) and fluorescence spectra (c) of EtOH/water mixed solution of **L** in different pH.

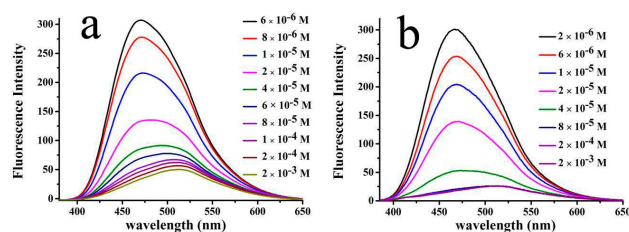


Fig.7 Fluorescence spectra of **L-Tm** (a), **L-Yb** (b) with different concentration of RE metal ions

aggregation of **L** molecules, another kind of RE ion, Yb^{3+} , was investigated. A completely different morphology compared with that of Tm^{3+} was observed as shown in Fig. 5. Moreover, the concentration of Yb^{3+} ion also influenced **L** aggregation mode. When the aqueous solution of Yb^{3+} (8×10^{-5} M) was used, flower-like nanorods structure was obtained, among which six nanorods extending in six directions revolved round the centre point (Fig. 5a) to form the six-branched flower. When the concentration of Yb^{3+} increased to 2×10^{-4} M, the length of the nanorods increased to $\sim 40 \mu\text{m}$ and the nanostructure gathered gradually (Fig. 5b). Also, to eliminate the hydrolysis effect, Yb^{3+} (6×10^{-5} M) was added in solution of pH = 3, regular hexagonal (Fig. 5c) and hexagonal prisms (Fig. S4) images can be observed with average side length being $2 \mu\text{m}$. These hexagonal flakes were believed the gem of the flower-like six-branched structures.

3.5 Linear optical properties and theoretical calculation

3.5.1 Linear optical properties in different acidity solutions

The UV-vis absorption spectrum of **L** in EtOH solution exhibited two major absorption bands centred at 293 nm and 364 nm (Fig. 6a), respectively. The latter corresponded to the π - π^* transition of the whole **L** molecule, while the former resulted from the triphenylamine fragment [32]. To further investigate the molecular level, and to better understand the relationship between the optical properties and electronic structure of **L**, theoretical calculations on the energy levels were performed by TD-DFT method at pbe1pbe/6-31g level based on the molecule conformation in the crystal structure [33]. In the highest occupied molecular orbital (HOMO), the electrons were mainly concentrated on the electron-donating triphenylamine moiety

with low coefficients on the electron-withdrawing cyanovinyl group. While in the lowest unoccupied molecular orbital (LUMO) plots, the electrons were mainly located on the electron-withdrawing groups. The separation between HOMO and LUMO indicated that substantial charge transfer from the donor moiety to the acceptor moiety occurred when molecules were excited.

Further, the theoretical spectral characteristic showed two main transitions. One was from the configuration HOMO to LUMO with $\lambda_{\text{abs}} = 367$ nm (oscillator strength $f_{\text{HOMO-LUMO}}$ being 0.6745). The other optical transition corresponded to the configuration HOMO to LUMO+1 with $\lambda_{\text{abs}} = 296$ nm. The calculated results fit with the experimental data and the corresponding absorption bands are observable on the absorption spectra of **L**-EtOH solution.

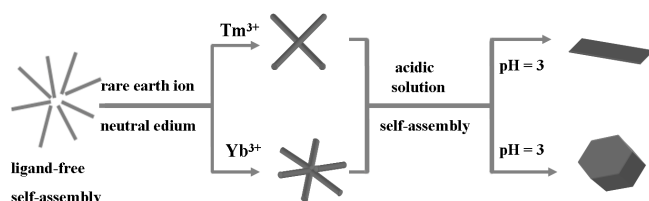
Further, UV-vis absorption spectra of **L** nanostructures obtained in different acidity aqueous solutions were thoroughly studied. The results revealed that the π - π^* transition of the whole conjugated structure changed a little with the change of the acid and alkali environment. The absorption band centred at 362 nm in acidic solution of pH = 1 and/or 3, which was 356 nm in the neutral environment of pH = 7 while it centred at 359 nm in alkaline solution of pH = 13. At the same time, the absorption band from triphenylamine fragment varied much more, which centred at 284 nm, 293 nm and 300 nm in acidic, neutral and alkaline solution, respectively. Moreover, the ratio of the two peak value showed fluctuation. In acidic solution of pH = 1 and 3, the absorbance ratio of A_{284}/A_{362} was 0.3768, where the suffix represents the monitor wavelength. In neutral solution of pH = 7, the absorbance ratio of A_{293}/A_{365} increased to 0.5687. In alkaline solution of pH = 13, the absorbance ratio showed a further increase to $A_{300}/A_{359} = 1.0869$. The results meant that the electronic structure of the whole conjugated structure changed little with the different acidity of the solution. The phenomenon was reasonable that the acidity of the solution changed the H atom of carboxylic group, which was not included in the whole conjugated structure. On the other hand, the different acidity of the solution violently influenced the electronic structure of the triphenylamine fragment. The higher the acidity was, the more the influence occurred.

As for the fluorescence emission, there was a stable blue-shift wavelength band varied from acidic conditions to alkaline medium, and then to alkaline medium. When the pH value of the solution was 1, the emission band centred at 484 nm. When the pH value increased to 7, the emission band blue-shifted for about 9 nm to 475 nm, which further blue-shifted for about 23 nm to 461 nm as pH = 13. The results meant that there was a great environmental influence on the fluorescence with the increased pH value.

The changes of absorption and emission spectra in different acidity solutions indicated that, to a certain extent, the intermolecular interactions between **L-L** molecules and/or **L-solvent** were different in the acid-base aqueous solution environment, as mentioned above, which then brought about significant changes in morphology, size and optical properties.

3.5.2 Linear optical properties of **L-RE** nano hybrids

In addition, from the results and discussions mentioned above, the interactions between RE metal ions and **L** molecules were somewhat strong and could bring about significant changes in



Scheme 2 Possible formation mechanisms of **L** and RE metal ions nano/submicrocrystals with multimorphologies and size.

5 morphology and/or size. Besides the morphology/size research, a more important goal in this work was to investigate the effect of the interactions on the optical properties (Fig. 7). The maximum fluorescence emission band of **L**-EtOH solution was observed at 450 nm when it was excited at 360 nm. As was expected, when a small amount of Tm^{3+} ($6 \times 10^{-6} \text{ mol}\cdot\text{L}^{-1}$) was introduced to synthesize **L**- Tm nanohybrid (the ratio of **L** to Tm^{3+} was 167 : 1 at this moment), the emission showed a significant red-shift to 470 nm with quenched intensity. In the presence of Tm^{3+} ions, the heavy atom effect and the energy transfer from **L** to Tm^{3+} ions in the process of f-f transition may cause the fluorescence quench [34]. The red-shift might arise from the coordination effect between **L** and Tm^{3+} ions. The action 'hot spot' was O atoms of the carboxyl group, which was the electron-acceptor unit of **L**. The interactions may influence the electron distribution of **L**, increased the electron cloud density of the carboxyl group and further increased the strength of D-A pair, the direct result of which was the red-shift of the fluorescence.

As the usage of Tm^{3+} increased, the fluorescence quenched regularly. Along with this quenched emission, a more interesting phenomenon appeared. When the concentration increased to $2 \times 10^{-5} \text{ M}$ (the ratio of **L** to Tm^{3+} was 50 : 1), the fluorescence wavelength showed a wide emission peak, which centred at 470 nm with a shoulder peak at 513 nm. To further increase the concentration, the shoulder peak became more dominant. When the concentration increased to $2 \times 10^{-3} \text{ M}$ (the ratio of **L** to Tm^{3+} was 1 : 2), the fluorescence band mainly centred at 513 nm. After this point, the emission band and the fluorescence intensity did not change any more.

The emission band at 513 nm can be considered as the inherent fluorescent emission of **L**- Tm complex. When a small amount of Tm^{3+} was used, either the proportion of **L**- Tm complex was very small in the solution or the **L**- Tm complex had not yet been generated. Thus, the fluorescence showed only a red-shift emission. As increasing the usage of Tm^{3+} ions, the strong coordination ability emerged and the inherent fluorescent emission at 513 nm appeared. When the concentration of added Tm^{3+} ions increased to $2 \times 10^{-3} \text{ M}$, the ratio of Tm^{3+} to **L** was 2 : 1 at this condition. At this point, all of the **L** molecules may be coordinated with Tm^{3+} ions according to the results mentioned in SEM analysis. After this point, little change could be observed of the emission band and the fluorescence intensity. The results further confirmed the optimum ratio of Tm^{3+} to **L** was 2 : 1 in this study. To achieve the perfect coordination of Tm atom, some of water molecules may be involved in coordination effect.

The fluorescence property of **L**-Yb nanocomplex was similar to that occurred for **L**- Tm . With the increasing concentration of Yb^{3+} , the emission was gradual quenched. When the

concentration was $2 \times 10^{-6} \text{ M}$ (the ratio of **L** to Yb^{3+} was 500 : 1), there appeared an emission band centred at 467 nm, which red-shifted for about 17 nm compared to that of **L**-EtOH solution. When the concentration increased to $8 \times 10^{-5} \text{ M}$ (the ratio of **L** to Yb^{3+} was 12.5 : 1), the emission band at 467 nm disappeared, a new band centred at 515 nm appeared and the fluorescence intensity reached the minimum. Further, the emission band and the fluorescence intensity did not change any more when the concentration continually increased.

In terms of the mechanism, the driving forces for the formation of **L**-RE probably related to several kinds of forces, such as RE ions induced changing of intermolecular interactions and the corresponding crystal growth process, because X-ray powder diffraction (XRD) patterns of the three samples (Fig. S5) showed slight variations, such as the marked parts. Based on the results, the possible conversion process was illustrated in Scheme 2. In this process, when RE ions were introduced, metal ions influenced the intermolecular interactions of **L** molecules and further changed the crystal growth mode of them. When the usage of RE ions increased, the trend of change increased to result in **L**-RE nanohybrids [35]. Moreover, different RE ions had different influencing model. Thus, the crystal growth can be controlled by altering the species of RE ion, which resulted in crystals with different size and morphology. On the basis of the above analysis and SEM results, the possible conversion process may be as follows.

When Tm^{3+} was used, there was a tendency of **L** molecules grew along four different directions and aggregated to form the cross-morphology. Under the acidic conditions, the molecular interaction of carboxylic group and the Tm^{3+} was restrained due to protonation, resulting in the receded force and the unordered rectangular structures of nanoplates formed. As the concentration increased, the force of particular direction enhanced to grow into a large size sheet-like nanostructure finally.

Similarly, Yb^{3+} ions can induce **L** molecules grow along six different directions to form a hexagonal structure. The as-prepared hexagonal particles could serve as seeds to guide the subsequent growth of **L**-Yb to form the branched structures. To understand the formation process of the unique **L**-Yb architecture, intermediates of the product were traced. The existence of considerable hexagonal flakes was observed as typically shown in Fig. 5c. These hexagonal flakes were believed the gem of the six-branched **L**-Yb structures. The branched structure was formed from crystalline growth of the tiny particles along six high-surface-energy angle sections of the hexagonal sheet.

4. Conclusion

In this work, the self-aggregation of fluorophore-triphenylamine (**L**) nanostructures was studied in different conditions, including different solvent, different acidity of the solution, and under guide with RE ions Tm^{3+} and/or Yb^{3+} . The results revealed that controlled synthesis of self-assembled organic materials can be realized through changing the growing environment, which can also optimize the optical properties. This type of controlled synthesis method also opens up the possibility of utilizing the organic nanomaterial for a multitude of applications in bio- and chemical sensing and nanoelectronics.

Acknowledgements

This work was supported by the NSFC (No: 21101001, 21271004, 51372003), the Natural Science Foundation of Anhui Province (1208085MB22).

Notes and references

- † Electronic Supplementary Information (ESI) available: Selected bond lengths [Å] and angles [°] for **L**; The packing diagram of **L**; SEM image of **L** nanostructures prepared in pH = 4; SEM image of nanostructures of **L** with the excess concentration of Tm³⁺; SEM image of hexagonal prisms nanostructures when the Yb³⁺ was added to acidic aqueous solution of pH = 3.
- ‡ Crystallographic data reported in this manuscript were deposited with Cambridge Crystallographic Data Centre as supplementary publication No. CCDC-976845. These data can be obtained free of charge via <http://www.ccdc.cam.ac.uk/conts/retrieving.html>, or email: deposit@ccdc.cam.ac.uk
- 1 Y. S. Zhao, A. D. Peng, H. B. Fu, Y. M. Ma, J. N. Yao, *Adv. Mater.*, 2008, **20**, 1661-1665.
 - 2 H. B. Fu, B. H. Loo, D. B. Xiao, R. M. Xie, X. H. Ji, J. N. Yao, B. W. Zhang, L. Q. Zhang, *Angew. Chem., Int. Ed.*, 2002, **41**, 962-965.
 - 3 D. H. Kim, D. Y. Lee, H. S. Lee, W. H. Lee, Y. H. Kim, J. I. Han, K. Cho, *Adv. Mater.*, 2007, **19**, 678-682.
 - 4 J. G. Yu, F. R. F. Fan, S. L. Pan, V. M. Lynch, K. M. Omer, A. J. Bard, *J. Am. Chem. Soc.*, 2008, **130**, 7196-7197.
 - 5 K. Takazawa, Y. Kitahama, Y. Kimura, G. Kido, *Nano Lett.*, 2005, **5**, 1293-1296.
 - 6 A. L. Briseno, S. C. B. Mannsfeld, X. M. Lu, Y. J. Xiong, S. A. Jenekhe, Z. N. Bao, Y. N. Xia, *Nano Lett.*, 2007, **7**, 668-675.
 - 7 Y. B. Wang, H. B. Fu, A. D. Peng, Y. S. Zhao, J. S. Ma, Y. Ma, J. J. Yao, *Chem. Commun.*, 2007, 1623-1625.
 - 8 A. P. H. J. Schenning, E. W. Meijer, *Chem. Commun.*, 2005, 3245-3258.
 - 9 D. W. P. M. Löwik, I. O. Shklyarevskiy, L. Ruizendaal, P. C. M. Christianen, J. C. Maan, J. C. M. van Hest, *Adv. Mater.*, 2007, **19**, 1191-1195.
 - 10 H. Katagi, H. Kasai, S. Okada, H. Oikawa, H. Matsuda, H. Nakanishi, *J. Macromol. Sci., Pure Appl. Chem.*, 1997, **34**, 2013-2024.
 - 11 H. Nakanishi, H. Katagi, *Supramol. Sci.*, 1998, **5**, 289-295.
 - 12 T. Onodera, T. Oshikiri, H. Katagi, H. Kasai, S. Okada, H. Oikawa, M. Terauchi, M. Tanaka, H. Nakanishi, *Cryst. Growth.*, 2001, **229**, 586-590.
 - 13 X. L. Qiao, Z. J. Zhang, *Journal of Photochemistry and Photobiology A: Chemistry*, 2007, **190**, 15-21.
 - 14 G. Jia, K. Liu, Y. H. Zheng, Y. H. Song, M. Yang, H. P. You, *J. Phys. Chem. C.*, 2009, **113**, 6050-6055.
 - 15 J. Yang, C. X. Li, Z. W. Quan, C. M. Zhang, P. P. Yang, Y. Y. Li, C. C. Yu, J. Lin, *J. Phys. Chem. C.*, 2008, **112**, 12777-12785.
 - 16 S. Q. Ma, X. S. Wang, D. Q. Yuan and H. C. Zhou, *Angew. Chem., Int. Ed.*, 2008, **47**, 4130-4133.
 - 17 B. L. Chen, L. B. Wang, F. Zapata, G. D. Qian and E. B. Lobkovsky, *J. Am. Chem. Soc.*, 2008, **130**, 6718-6719.
 - 18 K. M. L. Taylor, J. D. Rocca, R. C. Huxford and W. B. Lin, *Chem. Commun.*, 2010, **46**, 5832-5849.
 - 19 R. Si, Y. W. Zhang, L. P. You, C. H. Yan, *Angew. Chem., Int. Ed.*, 2005, **44**, 3256-3260.
 - 20 Y. W. Zhang, X. Sun, R. Si, L. P. You, C. H. Yan, *J. Am. Chem. Soc.*, 2005, **127**, 3260-3261.
 - 21 Y. Li, F. K. Zheng, X. Liu, W. Q. Zou, G. Cong, C. Z. Lu, J. S. Huang, *Inorg. Chem.*, 2006, **45**, 6308-6316.
 - 22 Y. B. Song, C. A. Di, X. D. Yang, S. P. Li, W. Xu, Y. Q. Liu, L. M. Yang, Z. G. Shuai, D. Q. Zhang, D. B. Zhu, *J. Am. Chem. Soc.*, 2006, **128**, 15940-15941.
 - 23 Y. T. Tao, Q. Wang, L. Ao, C. Zhong, C. L. Yang, J. G. Qin, D. G. Ma, *J. Phys. Chem. C.*, 2010, **114**, 601-609.
 - 24 M. Faccini, M. Balakrishnan, M. B. J. Diemeer, Z. P. Hu, K. Clays, I. Asselberghs, A. Leinse, A. Driessen, D. N. Reinhoudt, W. Verboom, *J. Mater. Chem.*, 2008, **18**, 2141-2149.
 - 25 R. S. Moog, D. D. Kim, J. J. Oberle, S. G. Ostrowski, *J. Phys. Chem. A*, 2004, **108**, 9294-9301.
 - 26 D. Gudeika, A. Michaleviciute, J. V. Grazulevicius, R. Lygaitis, S. Grigalevicius, V. Jankauskas, A. Miasojedovas, S. Jursenas, G. Sini, *J. Phys. Chem. C*, 2012, **116**, 14811-14811.
 - 27 G. M. Sheldrick, *SHELXTL V.51 Software Reference Manual*, Bruker AXS, Inc., Madison, Wisconsin, USA, 1997.
 - 28 M. J. G. W. T. Frisch, H. B. Schlegel, G. E. Scuseria, M. A. Robb, J. R. Cheeseman, G. Scalmani, V. Barone, B. Mennucci, G. A. Petersson, H. Nakatsuji, M. Caricato, X. Li, H. P. Hratchian, A. F. Izmaylov, J. Bloino, G. Zheng, J. L. Sonnenberg, M. Hada, M. Ehara, K. Toyota, R. Fukuda, J. Hasegawa, M. Ishida, T. Nakajima, Y. Honda, O. Kitao, H. Nakai, T. Vreven, J. A. Montgomery, Jr, J. E. Peralta, F. Ogliaro, M. Bearpark, J. J. Heyd, E. Brothers, K. N. Kudin, V. N. Staroverov, R. Kobayashi, J. Normand, K. Raghavachari, A. Rendell, J. C. Burant, S. S. Iyengar, J. Tomasi, M. Cossi, N. Rega, J. M. Millam, M. Klene, J. E. Knox, J. B. Cross, V. Bakken, C. Adamo, J. Jaramillo, R. Gomperts, R. E. Stratmann, O. Yazyev, A. J. Austin, R. Cammi, C. Pomelli, J. W. Ochterski, R. L. Martin, K. Morokuma, V. G. Zakrzewski, G. A. Voth, P. Salvador, J. J. Dannenberg, S. Dapprich, A. D. Daniels, O. Farkas, J. B. Foresman, J. V. Ortiz, J. Cioslowski and D. J. Fox, Gaussian 09, Revision B.01, Gaussian, Inc., Wallingford CT, 2009.
 - 29 L. J. Prins, D. N. Reinhoudt and P. Timmerman, *Angew. Chem., Int. Ed.*, 2001, **40**, 2382-2426.
 - 30 T. Y. Wang, J. Jiang, Y. Liu, Z. B. Li, M. H. Liu, *Langmuir.*, 2010, **26**, 18694-18700.
 - 31 T. Imae, Y. Takahashi, H. Muramatsu, *J. Am. Chem. Soc.*, 1992, **114**, 3414-3419.
 - 32 X. L. Tang, W. M. Liu, J. S. Wu, C. S. Lee, J. J. You, P. F. Wang, *J. Org. Chem.*, 2010, **75**, 7273-7278.
 - 33 (a) H. D. Ju, X. T. Tao, Y. Wan, J. H. Shi, J. X. Yang, Q. Xin, D. C. Zou, M. H. Jiang, *Chem. Phys. Lett.* 2006, **432**, 321-325; (b) Z. Zheng, Q. Zhang, Z. P. Yu, M. D. Yang, H. P. Zhou, J. Y. Wu, Y. P. Tian, *J. Mater. Chem. C.*, 2013, **1**, 822-830.
 - 34 S. Bano, A. Mohd, A. A. P. Khan, K. S. Siddiqi, *J. Chem. Eng. Data.*, 2010, **55**, 5759-5765.
 - 35 J. Liu, B. Xu, C. Song, H. D. Luo, X. Zou, L. X. Han, X. B. Yu, *CrystEngComm.*, 2012, **14**, 2936-2943.